

# Controller Design for Polymer Electrolyte Membrane Fuel Cell Systems for Automotive Applications

Juan Carlos Gómez<sup>a</sup>, Maria Serra<sup>a</sup>, Attila Husar<sup>a</sup>

<sup>a</sup>Institut de Robòtica Informàtica i Industrial CSIC-UPC

C. Llorens i Artigas 4-6, 08028, Barcelona, Spain.

e-mail address of corresponding author: maria.serra@upc.edu

phone number of corresponding author: +34934015751

fax number of corresponding author: +34934015750

---

## Abstract

Continuous developments in Proton Exchange Membrane Fuel Cells (PEMFC) make them a promising technology to achieve zero emissions in multiple applications including mobility. Incremental advancements in fuel cells materials and manufacture processes make them now suitable for commercialization. However, the complex operation of fuel cell systems in automotive applications has some open issues yet. This work develops and compares three different controllers for PEMFC systems in automotive applications. All the controllers have a cascade control structure, where a generator of setpoints sends references to the subsystems controllers with the objective to maximize operational efficiency. To develop the setpoints generators, two techniques are evaluated: off-line optimization and Model Predictive Control (MPC). With the first technique, the optimal setpoints are given by a map, obtained off-line, of the optimal steady state conditions and corresponding setpoints. With the second technique, the setpoints time profiles that maximize the efficiency in an incoming time horizon are continuously computed. The proposed MPC architecture divides the fast and slow dynamics in order to reduce the computational cost. Two different MPC solutions have been implemented to deal with this fast/slow dynamics separation. After the integration of the setpoints generators with the subsystems controllers, the different control systems are tested and compared using a dynamic detailed model of the automotive system in the INN-BALANCE project running under the New

European Driving Cycle.

*Highlights:* The control structure of a PEM fuel cell system in an automotive application is described. An off-line optimal setpoint generator is compared to MPC techniques. Slow and fast dynamics are split in the MPC design for computational burden reduction. Simulations are based on a model tuned using experimental data from a real automotive fuel cell system.

*Keywords:* Automotive application, Control structure, Efficiency optimization, Fuel cell system, Non-linear Model Predictive Control

---

## 1. Introduction

Proton Exchange Membrane Fuel Cells (PEMFC) have many advantages that make them an interesting technology. In the automotive sector, they can displace fossil fuels. PEMFC are fed by hydrogen, that has one of the highest specific energy values, being three times higher than gasoline; their only byproduct is water, avoiding air pollution at all times; and they have efficiencies intrinsically higher than that of combustion engines [1]. Moreover, they are compact, have fast dynamics and a wide range of operating power.

Despite the advantages, fuel cells are not yet broadly used. One reason is that the fuel cell technology is still expensive. On the other hand, the hydrogen infrastructure is still insignificant compared to the infrastructure of other market competitors such as pure electric vehicles or gas vehicles.

This work arises from the European Union (EU) initiative to research and develop alternative solutions to current fossil-fuel-based mobility and from the European project INN-BALANCE, that focuses on the PEM fuel cell technology for automotive applications [2].

The main objective of the INN-BALANCE project is to boost hydrogen mobility by developing a new generation of highly-efficient fuel cell Balance of Plant (BoP) components. These components will add up to an innovative fuel cell system that greatly improve the efficiency and the reliability of fuel cell powered vehicles, while reducing their cost.

In PEMFC powered vehicles, the fuel cell system control is one of the most important elements to achieve efficiency improvements. In the literature, many studies addressing fuel cells control design can be found, as collected in [3]. Initial linear PID controllers were improved in different ways, such as the combination with feedforward control of stoichiometry or the application of

robust control [4]. However, PID controllers were overcome with model-based controllers. For this, control oriented models that describe the main system dynamics without excessive computational burden were needed, as the one presented in [5]. The use of first principles models is preferred in order to have a better understanding of the system behaviour. However, first principles models can easily deviate from real behaviour or become outdated. To solve these problems, several studies have presented state observers to estimate PEMFC non-measurable variables [6] and on-line parameters identification methods [7].

Model Predictive Control (MPC) is a model-based control methodology applied to PEMFC by several authors. In some cases, a linearized model was used [8]. However, non-linear MPC is required if the system has to operate at a wide range of load powers, as shown with experimental validation in [9] and [10]. On the other hand, distributed parameter models have been defended as necessary to properly describe distributed problems such as starvation. These distributed phenomena is relevant for the modelization of degradation [11]. Non-linear MPC with distributed model is therefore a promising control strategy [12]. However, it is difficult to implement because of the high number of unknown parameters and the computational burden. One way to reduce the number of unknown parameters is to implement a hybrid model combining data driven and physical models as described in [13], at the cost of losing the properties of the physical phenomenons occurring inside the fuel cell.

In automotive applications, the control structure is not straightforward. Controllers will be normally distributed at the lower level according to different subsystems objectives. These controllers will receive orders (setpoints) from a supervisory controller which may assume optimisation tasks. Moreover, in the vehicles, there are different operating modes (run mode, start up, shut down, etc.) which need to be treated differently. Up to now, only very few studies describe the controller's architecture of PEMFC systems in automotive applications. One example is found in [14].

In order to improve the performance of PEMFC vehicles, apart from optimizing the operation of the PEMFC system, it is important to optimize the overall energy management, including the energy storage elements. In the literature several works address the optimal power management of different kind of PEMFC hybrid vehicles. The authors in [15] describe the power management strategy of a hybrid tram powered by a PEMFC, a lithium-ion battery pack and a ultracapacitor pack for the minimisation of the hydrogen

consumption. In [16], a power management strategy based on Stochastic Dynamic Programming has been presented to optimize the efficiency. Using the same stochastic method, the degradation minimisation objective has been added to the efficiency minimisation in [17]. Moreover, a multi-objective design exploration is done in [18] to study the effect of the hybrid system elements sizing. Recently, the robustness of the energy management strategy facing uncertain driving cycles is shown in [19].

This work describes the control architecture of an automotive PEMFC system and develops three different supervisory controllers. Each one of the three supervisory controllers are in charge of coordinating the PEMFC subsystems and provide a unique interface from the vehicle to the PEMFC power system during run mode. This is done by converting the PEMFC power demand into the references required by the subsystems controllers. The supervisory controllers are based on non-linear models and compute optimal setpoints either by offline or online optimizations. Then, the local controllers of the subsystems manipulate the physical actuators according to their control laws and mechanisms. The power management between the PEMFC and the batteries is out of the scope of this work.

The proposed controllers performance is shown through simulation using the New European Driving Cycle (NEDC). The model parameters fit real experimental data corresponding to the INN-BALANCE project fuel cell system prototype.

The rest of this paper is organized as follows. In the second section, the system is described in terms of its subsystems and control architecture. The control objectives and the main restrictions are presented in the third section. In section four, the offline setpoint generator technique is presented and developed. In section five, two non-linear MPC are developed based on this case study. Section six presents the results and a comparative analysis of the three proposed setpoint generators. Finally, in the last section, the main conclusions of the work are drawn.

## 2. System Description

The automotive fuel cell system studied in this work, developed for the INN-BALANCE project, has a PEMFC stack and three subsystems, namely the cathode subsystem, the anode subsystem and the thermal subsystem. The cathode subsystem feeds oxygen in the form of compressed humidified air into the cathode inlet of the fuel cell stack. Similarly, the anode subsystem

feeds compressed hydrogen from the tank into the anode inlet. The thermal subsystem is required to control the operating temperature of the fuel cell. The main characteristics of the fuel cell system are:

- 100 kW gross power fuel cell stack
- 300 cm<sup>2</sup> of active area PEM fuel cells
- 335 cells
- 450 A maximum operating current, 1.5 Acm<sup>-2</sup>
- 550 A peak current, only for few seconds
- 30 A minimum current
- 12 kW compressor in the cathode subsystem with a maximum mass flow of 120 gs<sup>-1</sup>
- Passively humidified cathode (wet side of humidifier fed with cathode outlet stream)
- Hydrogen surplus re-circulation in the anode
- Thermal subsystem composed by different cooling modules

### 2.1. Control Architecture

The control architecture designed for the PEMFC system has several layers in order to manage the system operation at different levels. In the top layer there is the state machine, which is in charge of activating one among different operation modes and submodes and determines the discrete states of the system. The main operation modes are: INITIAL, RUN, STARTUP, FREEZE STARTUP, SHUTDOWN and FREEZE SHUTDOWN. The optimal setpoint generator of this work is part of the state machine and it is designed to work during the run mode.

The global control architecture is presented in Figure 1. As it is shown, the control actions are computed in the Control Unit, which follows a cascade control structure from the upper level to the local SubSystems Controllers (SSC). The state machine receives all the available information in the system from the input wrapper, including relevant driver actions, and signals from the sensors and observers. The state machine also receives information from

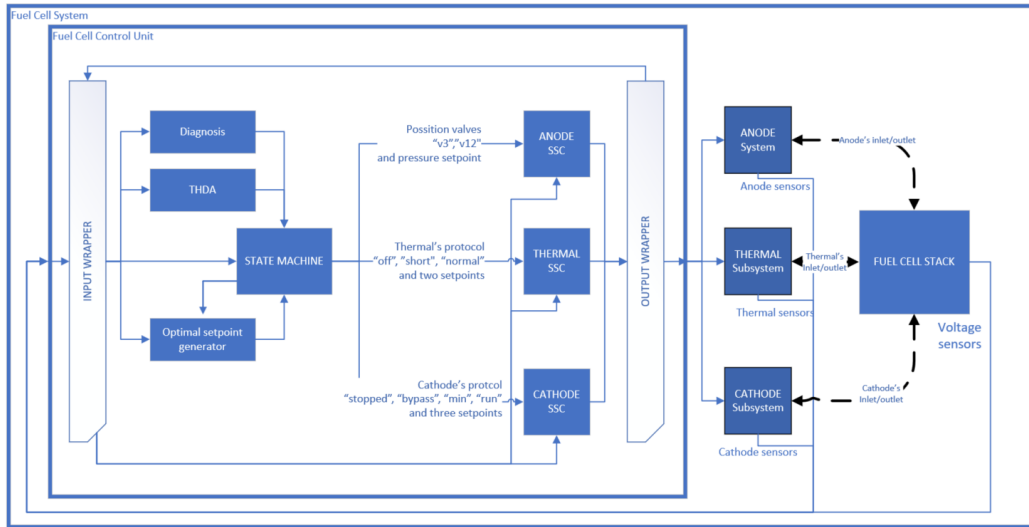


Figure 1: Fuel cell system control architecture

the optimal setpoint generator, the diagnosis system and the Total Harmonic Distortion Analysis (THDA) system. Each subsystem controller calculates the local control actions based on the sensors values and setpoints received from the state machine. The control actions are sent to the output wrapper which transmit them to the actuators.

The state machine also contains the conditions required to transit from one state to the other. Some state transitions are forbidden (e.g. from INITIAL to RUN modes it is necessary to pass through STARTUP). All transitions are triggered based on exogenous and internal signals to ensure operation safety and good use of the resources.

## 2.2. Cathode subsystem

The cathode subsystem, developed at Brose<sup>1</sup> together with its local controller, is in charge of delivering the required oxygen flux with the desired pressure and relative humidity. It is mainly composed of a compressor developed by Celeroton<sup>2</sup>, a heat exchanger, a passive humidifier, a three-way valve to control the flow of air into the humidifier and a back pressure valve. All

<sup>1</sup>Brose Mechatronics, Germany

<sup>2</sup>Celeroton AG, Switzerland

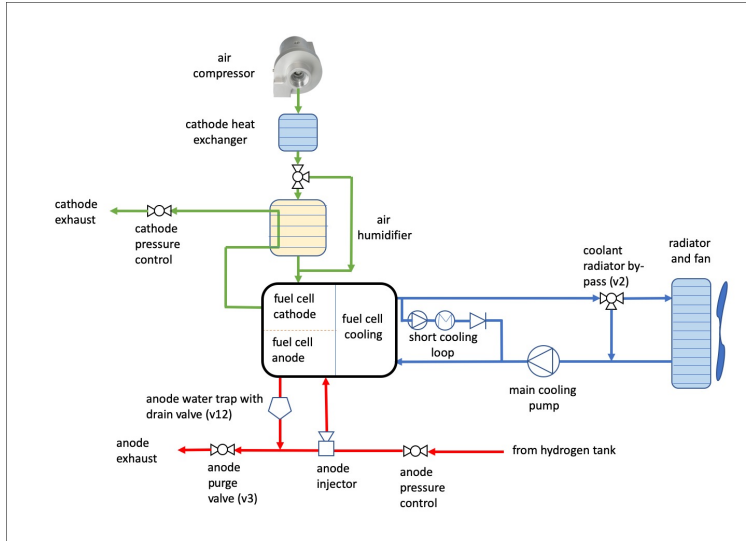


Figure 2: Fuel cell system physical scheme

these elements can be seen in the upper part of the system diagram shown in Figure 2.

The role of the cathode subsystem is key to efficiency. It has two main components. On the one hand, there is the compressor, which is powered from the internal DC bus and takes around 10% of the total gross power. On the other hand, there is the humidifier with its three-way valve. The three-way valve is able to direct the compressed air into the humidifier, to the bypass, or it can have any position in between, which makes the cathode inlet a mix of dry and wet air.

The back-pressure valve, active in the run mode, is a high frequency valve that can increase the gas flow dynamic resistance, controlling the pressure inside the fuel cell.

The thermal subsystem controls the temperature of the cathode subsystem with a heat exchanger. However, the thermal management of the cathode subsystem is out of the scope of this work.

During the run mode, the cathode subsystem controller receives three inputs (setpoints) from the setpoint generator:

- $r_1$ : Mass flow reference
- $r_2$ : Humidity ratio (by mass) reference

- $r_3$ : Inlet pressure reference

The cathode subsystem controller has additional inputs that are managed by the state machine and are used to configure the position of valves during modes like startup and shutdown.

### 2.3. Anode subsystem

The anode subsystem together with its local controller is developed at AVL<sup>3</sup> and it provides the flux of hydrogen from the  $H_2$  tank to the fuel cell. The anode subsystem controller controls the pressure on the anode inlet to be 0.2 bar above the pressure on the cathode inlet, in accordance to the fuel cell manufacturer's requirements.

The anode subsystem uses an injector-ejector unit to recirculate the  $H_2$  in order to minimize the losses. However, due to  $N_2$  crossover and that  $N_2$  is not consumed by the reaction, the  $N_2$  concentration tends to raise. For this reason, periodic purges are required to decrease the pressure and the concentration of  $N_2$  on the anode. The purges of the anode are made by opening the corresponding valve, indicated as v3 in Figure 2. Special attention is given to the gas purging valve because during the purge, both hydrogen and nitrogen are ejected to the exhaust. During this operation, the injector-ejector valve is open to maintain the pressure on the anode's channel. Hence, the purging valve is to be open just a short period of time to minimise the hydrogen lost to the atmosphere.

This subsystem is also equipped with a water trap which collects liquid water droplets from the anode's outlet. A liquid water drain valve, v12, discharges the water collected in the water trap.

During the run mode, the anode subsystem controller receives one input (setpoint):

- $r_4$ : Inlet anode pressure reference

When the car is not in the run mode, the state machine takes control of the anode subsystem valves.

### 2.4. Thermal subsystem

The fuel cell generates electricity and heat, and it is designed to run at the temperature range of 68 to 80 degrees Celsius. The temperature of the fuel

---

<sup>3</sup>AVL List GmbH, Engineering Service Provider

cell reaction affects significantly the efficiency. Hence, the fuel cell system contains a thermal subsystem to control the stack temperature. The thermal subsystem, developed by DLR <sup>4</sup>, also manages other thermal activities in the anode and cathode subsystems which are not included in this work, including the cathode heat exchanger.

The fuel cell is cooled with a liquid coolant, which can either pass through a normal circuit or a short startup circuit, as shown in Figure 2. The short circuit is only used during the freeze startup procedure. To control the coolant temperature, the thermal subsystem has a radiator, one main pump, and one three-way valve, indicated as v2 in Figure 2.

The coolant temperature is measured with two temperature sensors: one on the coolant inlet, and the other on the outlet to the stack. During normal operation of the system, the coolant inlet temperature has to be 68 degrees Celsius, and the coolant outlet temperature cannot be higher than 80 degrees. A minimum flow in the main pump is required to have good measurements of the coolant temperature.

Similarly to the cathode and anode subsystems, the thermal subsystem controller receives two references from the setpoint generator during the run mode. These are:

- $r_5$ : Inlet coolant temperature reference
- $r_6$ : Coolant temperature increment reference

The thermal subsystem controller has other inputs for the selection of the thermal system configuration, in charge of the state machine. During the run mode, the cooling circuit is always set to normal.

### *2.5. Load control device*

Finally, the fuel cell reaction is controlled by a load control device that can set the amount of electric current that comes from the fuel cell. The current manager, not presented in this work, sets the current of the fuel cell based on the car velocity, driver's throttle, and the state of charge of the battery.

---

<sup>4</sup>DLR Stuttgart, German Aerospace Center

### 2.6. Simulation Model

A dynamic system model that describes the behaviour of all the subsystems has been integrated. This model is used to simulate the system in the selected scenarios described later in this work. The stack model is a first principles isothermal distributed model based on [20] and described in [21], where 1D spatial discretization is implemented along the flow channels and where identical behaviour of all cells is assumed. Additionally, the simulation model used in this work includes the discretization of the cathode diffusion layer in the direction perpendicular to the membrane, as well as advanced methods to describe the water content in the membrane,  $\Lambda_C$ , and the water liquid fraction in the cathode catalyst layer,  $S$ , which makes the model accurate at a larger range of temperatures and relative humidities. The membrane water content, with an important effect on the membrane conductivity, has a dynamics given by the gradients of chemical potentials and protons, which determine the water fluxes through the membrane, as explained in [22]. The  $S$  dynamics is given by the evaporation rate and the liquid water generation terms, as described in [23]. This way, the important effect of the temperature on the hydration model is considered, as claimed by [24]. The implementation of the improved stack model is described in [12]. The thermal, anode and cathode subsystems models are lumped parameter models that are intellectual property of DLR, AVL and Brose, respectively. The model parameters have been tuned using experimental data from the fuel cell system of the INN-BALANCE project [25].

### 3. Control Objectives

The control objectives set in this work are the maximization of the system efficiency and the satisfaction of the constraints of the system during the run mode. The optimization decision variables are the references of the different subsystem controllers,  $r_1$  to  $r_6$ . However, the manufacturer's requirements fix  $r_5$  to 68 degrees Celsius and the anode inlet pressure,  $r_4$ , to be 0.2 bar above the cathode inlet pressure. Therefore, these two references are not actual decision variables, and the space of search is only defined by  $r_1$ ,  $r_2$ ,  $r_3$  and  $r_6$ .

### 3.1. System Efficiency

The global system efficiency,  $\eta$ , is defined taking into account all subsystems:

$$\eta = \frac{P_{net}}{P_{in}} = \frac{I \cdot V_{fc} - \sum_{s=\text{subsystems}} P_s}{HHV \cdot \dot{n}_{H_2}} \quad (1)$$

where  $\dot{n}_{H_2}$  is the fuel out of the  $H_2$  tank, and  $HHV$  is the hydrogen High Heating Value.  $IV_{fc}$  is the gross electrical power generated by the fuel cell and  $P_s$  is the electrical power consumed by the subsystems. The compressor consumption, modelled with information provided by Celeroton, can reach 12 kW and it is the main parasitic load, which varies with the operating conditions. The rest of the parasitic loads are assumed constant and will not be considered in this work. The largest of these minor parasitic consumptions corresponds to the thermal management module, and it is estimated at 1.9 kW.

### 3.2. Control Requirements and Constraints

In Table 1, the system requirements are presented. In addition to these constraints, for any current below 60 A, the PEMFC system has to use the mass flow corresponding to 60 A. This is necessary to ensure a good reactant distribution across the fuel cell. The fuel cell stack current, set by the current manager, is considered an exogenous known variable.

It is also worth mentioning that some constraints are not always possible to accomplish, e.g. the RH at the anode and cathode inlets. The cathode subsystem is humidified passively and for safety reasons during the shutdown it is dried out. Then shortly after startup, it is not possible that the system provides proper humidification.

Next, the requirements in Table 1 are applied to the different references in order to know how they are restricted during the run mode, which is indicated in Table 2:

1. The cathode mass flow reference not representing a stoichiometry of less than 1.6 yields  $r_1 \geq 1.6 \cdot \text{StoichiometricAirFlow} = 0.2121 \cdot I_{fc}$ . This condition, when applied to 60 A, gives 13.2 g/s, as indicated in Table 2.
2. The cathode inlet Relative Humidity (RH) being greater than 30% limits the inlet Humidity Ratio (HR) reference,  $r_2$ , accordingly. Assuming the inlet air is close to atmospheric pressure and the lowest inlet temperature of 68°C, then 30% RH corresponds to 0.031 HR, and at the

Table 1: Constraints on the fuel cell stack

Magnitude	Unit	Min	Max
Stoichiometry cathode	-	1.6	
Stoichiometry anode	-	1.4	
Cathode inlet RH	%	30	
Anode inlet RH	%	20	
Anode inlet press.	bar	$0.2 + P_{cath}$	$0.5 + P_{cath}$
Anode outlet press.	barG		2.2
Cathode outlet press.	barG		2
Coolant inlet temp.	°C	68	68
Coolant outlet temp.	°C	68	80
Current	A	30	450
Peak current (less 10 s)	A	10	570

highest inlet temperature of 80°C, 100% RH corresponds to 0.561 HR, as indicated in Table 2.

Table 2: Constraints on the generated setpoints

	Set-points	Unit	Min	Max
$r_1$	<b>Cathode mass flow</b>	$\text{gs}^{-1}$	13.2	-
$r_2$	<b>Cathode HR</b>		0.031	0.561
$r_3$	<b>Cathode inlet press.</b>	bar	$P_{amb}$	$P_{amb} + 2.2$
$r_4$	Anode inlet press.	bar	$P_{amb} + 0.2$	$P_{amb} + 2.4$
$r_5$	Coolant inlet temp	°C	68	68
$r_6$	<b>Coolant diff. temp</b>	°C	0	12

In Table 2, the setpoints that result from the optimization process have been highlighted.

#### 4. Offline Map-Based Controller

The idea behind this technique is to find the best possible steady state operating conditions for a list of currents. Then, the setpoints applied to the subsystems are based on a polynomial regression of the obtained results.

#### 4.1. Optimisation description

The offline optimum setpoint generator is a function of the current of the stack that tells the setpoint values that maximize the efficiency based on steady state conditions. Since  $r_4$  and  $r_5$  are already fixed by the manufacturer specifications, the setpoint generator computes only four outputs, which are  $r_1$ ,  $r_2$ ,  $r_3$  and  $r_6$ :

Off. gen. :  $\mathbb{R} \rightarrow \mathbb{R}^4$

Off. gen. :  $(I_{st}) \rightarrow (r_1, r_2, r_3, r_6)$

The optimisation problem is to find the set of setpoints that lead to the maximum efficiency given a current  $I_{st}$ :

$$\begin{aligned} & \underset{r=r_1, \dots, r_6}{\text{maximize}} && \eta(r)|_{I_{st}} \\ & \text{subject to} && \underline{r}_i \leq r_i \leq \bar{r}_i \\ & && \mathbf{A}r \leq \mathbf{B} \end{aligned} \tag{2}$$

where  $\eta$  is the efficiency,  $\underline{r}_i$  and  $\bar{r}_i$  are the lower and higher boundaries, and  $A$  and  $B$  are the inequality constraints. The inequality constraints are necessary to restrict the solution region to accomplish the compressor physical limits. These limits apply for  $r_1$  and  $r_3$  and will be explained in sections 5.2 and 5.3.

One well known approach in the optimization literature is the use of the Karush-Kuhn-Tucker conditions to solve and find the local and global maximum [26]. However, a requirement to use this technique is that the function to be maximized has to be known and continuously differentiable. Moreover, this technique can be tedious and error-prone if the function to optimize is too complex, as it is in this case. This is due to the fact that the integrated system model, object of our study, has more than one hundred states and does not have an explicit steady-state efficiency function.

Alternatively, in this section, a static offline map of the PEMFC system is made based on the simulation model. The input variables of this map are the fuel cell current and the subsystem references. The output of this map is the system efficiency.

Off. map :  $\mathbb{R}^5 \rightarrow \mathbb{R}$

Off. map :  $(r_1, r_2, r_3, r_6, I_{st}) \rightarrow (\eta)$

For each current, the stack model has been run under all the possible combinations of valid setpoints inside a finite four-dimensional grid (the orange dots in Figures 3 and 4) to get a full map of the system characteristics.

Table 3: Some Evaluated Optimal Setpoints I

Current [A]	$r_1 : m_{in}$ [gs <sup>-1</sup> ]	Cath. stoich.	$r_2$ : HR
60	33.779	3.6	0.412
100	31.276	2	0.374
150	49.26	2.1	0.311
200	62.312	2.1	0.267
250	72.377	1.9	0.232
300	86.612	2	0.204
350	95.994	1.9	0.158
400	98.16	1.8	0.133
450	107.18	1.8	0.100

In Figure 3, the obtained single cell voltages, stack power and system efficiency can be found as a function of current. The results of this process are validated with the original integrated model.

#### 4.2. Static Optimal References Results

The results of the offline optimisation can be found in Tables 3, 4 and 5, and are shown in Figures 3 and 4. Figure 4 shows the optimal references at every evaluated current and the regression function. It can be seen that the system constraints are taken into account.

To obtain the optimal reference set given the stack current,  $r^*(I_{st})$ , a regression into a 5th order polynomial of the data is done, shown with dashed lines in Figure 4. The coefficients of this polynomial can be found in the supplementary material.

$$r^*|_{I_{st}} = \left[ \begin{array}{c} r_1^* \\ r_2^* \\ r_3^* \\ r_6^* \end{array} \right] \Big|_{I_{st}} = \left[ \begin{array}{c} r_1^*(I_{st}) \\ r_2^*(I_{st}) \\ r_3^*(I_{st}) \\ r_6^*(I_{st}) \end{array} \right] \quad (3)$$

## 5. Nonlinear MPC

A second methodology is applied to find the optimal setpoints. In this case, the dynamics of the system is taken into consideration. The methodology is the Model Predictive Control. MPC is a predictive control technique

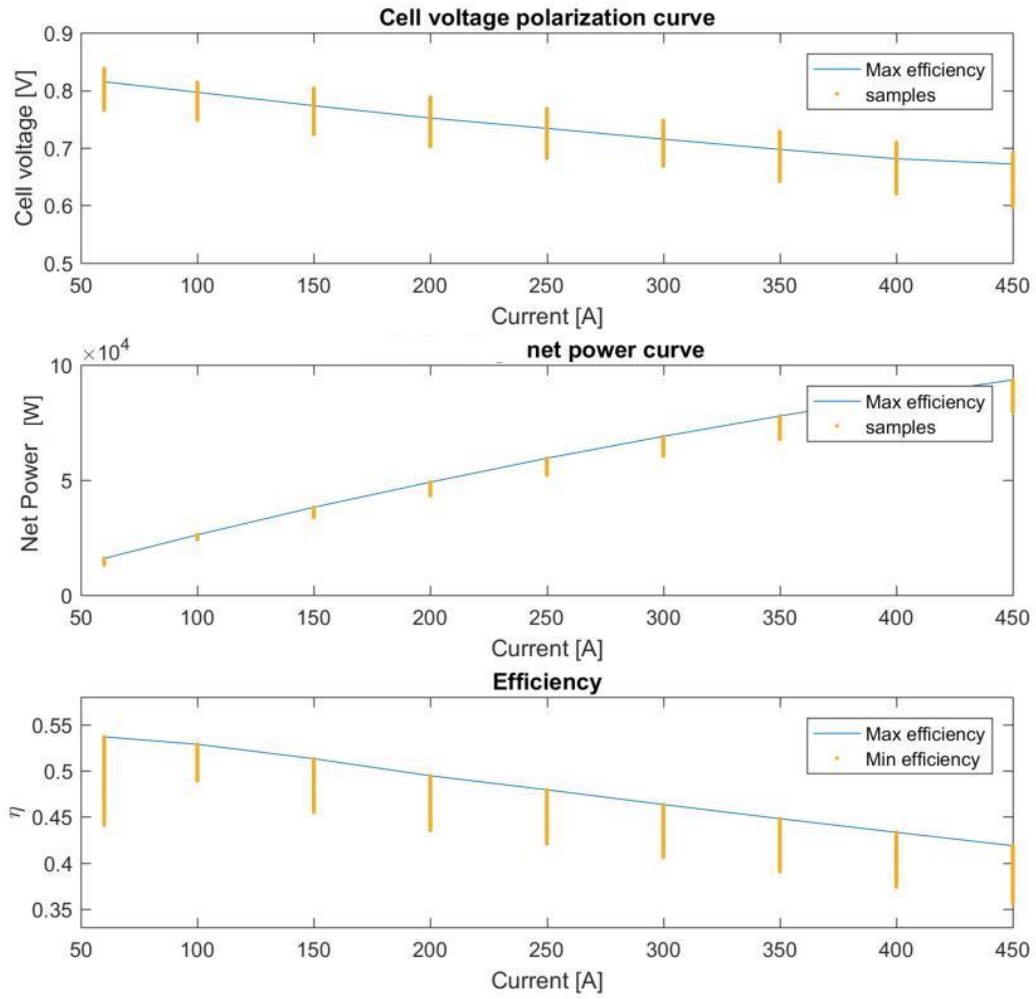


Figure 3: Polarization curve, Power curve and efficiency

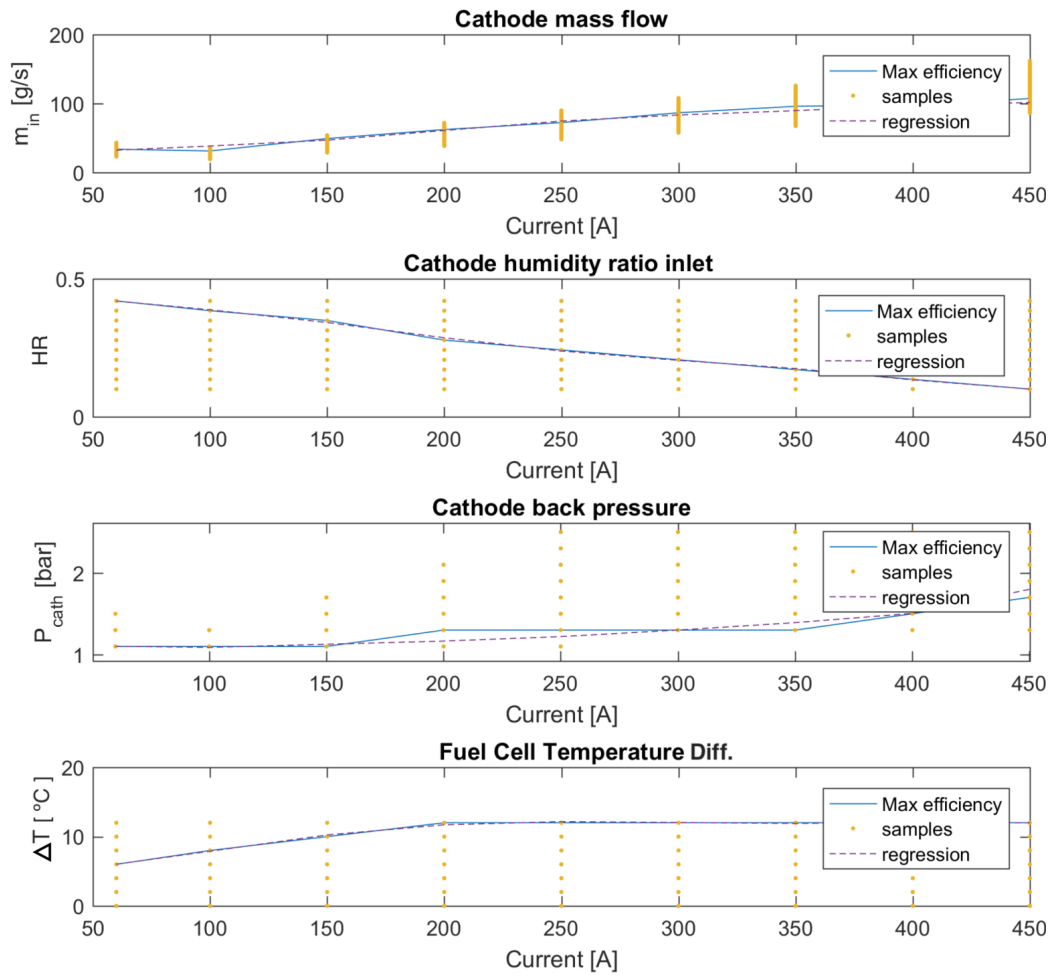


Figure 4: Best references at each current.

Table 4: Some Evaluated Optimal Setpoints II

Current [A]	$r_3 : P_{cath}$ [bar]	$r_6 : \Delta T$ [ $^{\circ}\text{C}$ ]
60	1.1	6
100	1.1	8
150	1.1	10
200	1.3	12
250	1.3	12
300	1.3	12
350	1.3	12
400	1.5	12
450	1.7	12

Table 5: Optimal Power at Evaluated Setpoints

Current [A]	$P_{\text{gross}}$ [kW]	$P_{\text{compressor}}$ [kW]	$P_{\text{net}}$ [kW]
60	16.223	0.3996	15.823
100	26.500	0.3661	26.134
150	38.704	0.6192	38.085
200	51.050	2.0367	49.014
250	61.775	2.4233	59.352
300	72.138	3.0515	69.086
350	81.400	3.5374	77.862
400	91.243	5.2498	85.993
450	101.000	7.5044	93.500

Table 6: MPCs implementation based on the cost function, constraints and control model.

MPC type	Cost function	Constraints	Control Model
Linear, time-invariant MPC	Quadratic	Linear	Linear
Gain-scheduling MPC	Quadratic	Linear	Nonlinear
Adaptive MPC	Quadratic	Linear	Nonlinear
Nonlinear MPC (case-I)	Any	Linear or NL	Nonlinear
Nonlinear MPC (case-II)	Nonlinear	Nonlinear	Linear

suitable for complex dynamical systems, that uses internal Control Oriented Models (COM) to predict and optimize the system outcome (cost function) based on the manipulated variables.

Model predictive controllers are usually classified by the type of cost function, constraints and control model, as shown in Table 6 [27]. The kind of MPC that suits better this project is the Nonlinear MPC (NMPC), and particularly, case-I. Indeed, the objective function is nonlinear, as explained in section 5.1; the control model is also nonlinear because this maintains the nonlinearities of the plant, as explained in section 5.2; and the constraints that bound the search region based on safety and manufacturer limits are nonlinear too, as explained in section 5.3.

In Figure 5, the control architecture of the predictive controller of this work is presented. The predictive controller outputs are the optimal setpoints of the subsystems local controllers. On the other hand, it is assumed that the predictive controller receives full state feedback of the system from the observers, as well as some other relevant exogenous variables such as the stack current.

The proposed architecture is divided into two NMPCs, one for the fast dynamics and the other for the slow dynamics, as shown in Figure 5. These two NMPCs have different control models, Manipulated Variables (MV), constraints and configuration. The idea behind decoupling the predictive controller into two is to reduce the computational cost of simulating the fast dynamics until the slow variables have an effect on the performance and are taken into account in the optimization.

The controller of the fast dynamics in the decoupled setpoint generator, NMPCFast, is mainly based on the cathode supply manifold behaviour. It is composed of the cost function  $J$ , the control model COM1, and the manipulated variables MV1 with their constraints. MV1 are the cathode mass flow

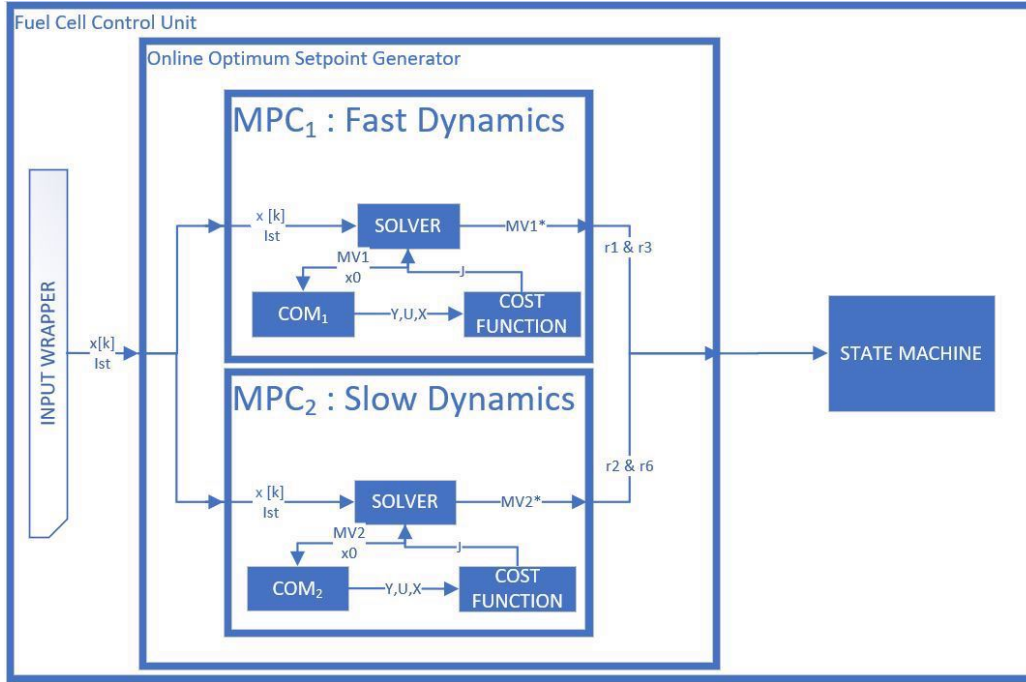


Figure 5: *Predictive controller II* architecture

reference,  $r_1 = u_1$ , and the cathode inlet pressure reference,  $r_3 = u_3$ .

The controller of the slow dynamics, NMPCSlow, is based on the behaviour of the temperature and the humidification. NMPCSlow is composed of the cost function  $J$ , the control model COM2, and the manipulated variables MV2 with their constraints. MV2 are the cathode humidity ratio reference,  $r_2 = u_2$ , and the coolant temperature increment reference,  $r_6 = u_6$ .

NMPCFast has a prediction horizon of 1 second and the control action is calculated every 0.1 seconds. The NMPCSlow, on the contrary, has a prediction horizon of 300 seconds and the control action is calculated every 2 seconds. The difference in more than two orders of magnitude is the main obstacle to having only one controller and model with all the dynamics.

### 5.1. Objective function

The nonlinear objective function  $J$  is used in both predictive controllers and represents the system efficiency. A negative sign is required to turn the

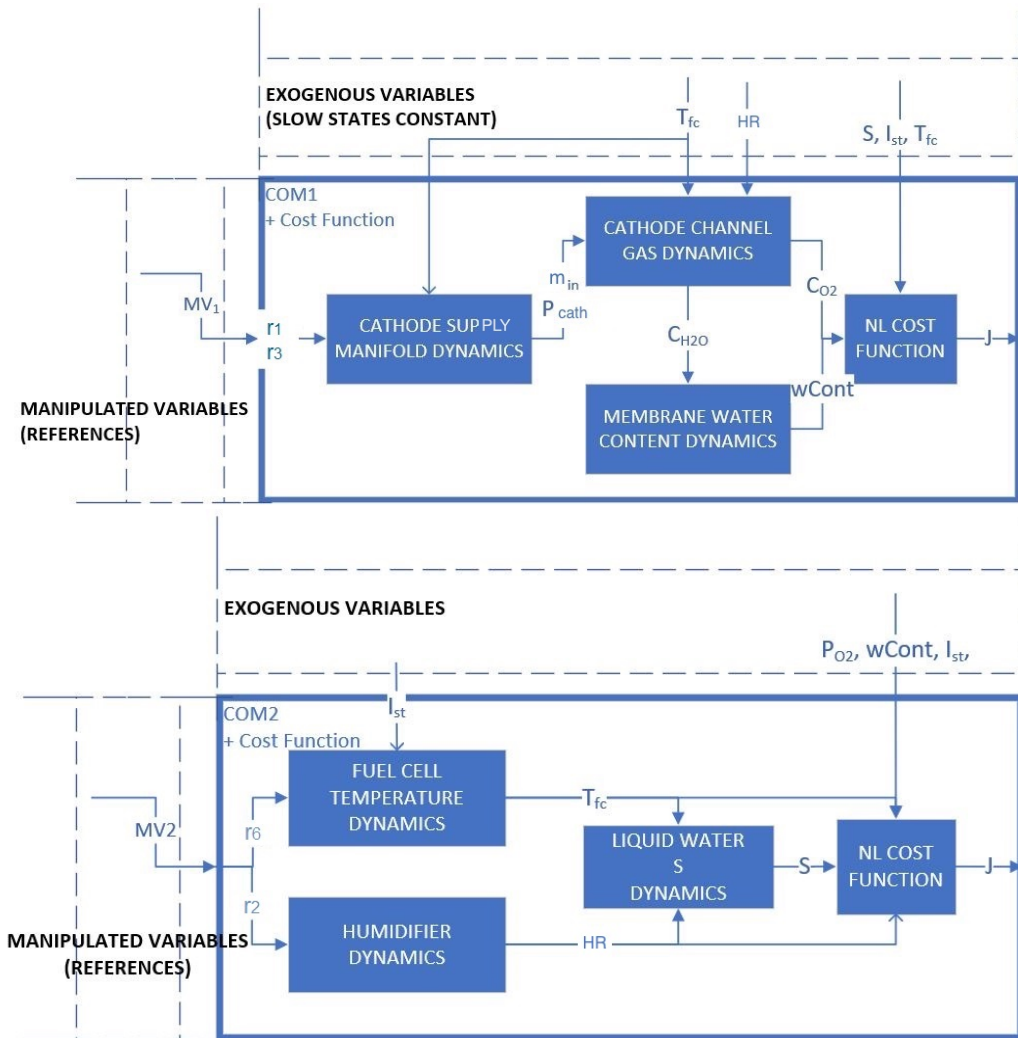


Figure 6: Control Oriented Models for the two Nonlinear MPCs

maximization problem into a minimization one, which is the solver input.

$$J = - \sum_k^M \left( \frac{P_{stack}[k] - P_s[k]}{HHV \cdot \dot{n}_{H2}[k]} \right)^2 \quad (4)$$

where  $P_{stack}[k] = I_{st}[k] \cdot V_{st}[k]$  is the power generated by the fuel cell at time  $k$ ,  $P_s[k]$  is the power consumed by the subsystems at instant  $k$ , assumed to be equal to the compressor consumption,  $\dot{n}_{H2}[k]$  is the hydrogen out of the tank at time  $k$ , and  $M$  is the prediction horizon.

### 5.2. Control models used in the MPC

The control models used in NMPCFast and NMPCSlow are based on simplified models of the PEMFC stack, cathode subsystem, anode subsystem and thermal subsystem. Moreover, COM1 contains the fast dynamics processes and COM2 the slow ones.

A scheme of the dynamics included in each COM is found in Figure 6. COM1 includes the cathode supply manifold dynamics, the fuel cell stack cathode channel concentration dynamics and the membrane water dynamics. COM1 considers that the humidity, temperature and liquid water are all constant.

Based on the simulation model of this work, the cathode fluid-dynamics is fitted into a 2x2 Multiple Input Multiple Output (MIMO) second order linear system, with the mass flow reference,  $r_1$ , and the inlet pressure reference,  $r_2$ , as inputs, and the actual variables values as outputs. The linearization is done around the point 50 g/s and 1.2 bar. Simulations of the resulting linear model and the original simulation model setpoint tracking behaviour are provided as supplementary material. In the stack, COM1 only keeps the cathode channel gas dynamics and the membrane water dynamics, as well as the spatial discretization has been eliminated. For the computation of the cost function, the nonlinear algebraic voltage expression of the simulation model is used, together with a static map of the compressor consumption. This map is a polynomial linear regression that gives the power consumed by the compressor as a function of the air mass flow and the cathode inlet pressure. The compressor working region, shown in Figure 7 is approximated with three polynomials: a second degree polynomial for the compressor bottom line, a third degree polynomial for the top surge line and a second degree polynomial for the top-down line in the region 95 g/s to 120 g/s. The coefficients of these polynomials are provided as supplementary material.

COM2 defines the slow dynamics of the fuel cell temperature, fuel cell humidity and liquid water, assuming that the fast variables are always equal to their setpoints.

The inputs of COM2 thermal model are the outlet coolant temperature reference,  $r_6$ , and the stack current,  $I_{st}$ , and the model output is the stack temperature,  $T_{fc}$ . The achievable stack temperatures under different currents have been determined using the simulation model. In this region, the thermal model is fit into a first order dynamic system with a time constant depending non-linearly on the current. This non-linear dependence has been adjusted with a 7th order polynomial. The simulations used to do this fitting are provided as supplementary material. The humidifier is modeled by a first order linear model relating the humidity ratio reference,  $r_2$ , with its actual value. The time constant of this model is 60 s. The dynamics of the liquid water fraction is kept as in the simulation model, but without the spatial discretization. The cost function block in COM2 is the same as in COM1.

### 5.3. Constraints

The constraints define the space of possible solutions of the problem. In this work, the constraints are defined to ensure safe operation and to reduce the search space of the solution.

#### 5.3.1. NMPCFast constraints

The references  $r_1$  and  $r_3$  are the cathode mass flow reference and the cathode inlet pressure reference. Figure 7 shows the references permitted region, which is defined by some lines that are used to keep the references inside the compressor limits. These lines are the compressor limit, the lower surge line and the upper surge line. Inside this region, at each time instant, the references constraints are updated based on the stack current.

*Upper and lower bounds.* At every time, a box is centered around the optimal setpoint found offline,  $r^*$ , which depends on the current. The upper bounds,  $UB_1$ , are specified as follows:

$$UB_1[k] = \begin{bmatrix} r_1^*(I_{st}[k]) + 10 \\ r_3^*(I_{st}[k]) + 0.25 \end{bmatrix} \quad (5)$$

The lower bounds,  $LB_1$ , are defined differently for  $r_1$  and  $r_3$ . The lower bound for  $r_1$  is the most restrictive between the offline optimal point minus

$10 \text{ gs}^{-1}$  and the minimum required stoichiometry (calculated as  $0.22 \cdot I_{st}$ ). In Figure 7, this limit is represented by the green dashed line.

$$LB_1[k] = \left[ \begin{array}{c} \max(0.22 \cdot I_{st}, r_1^*(I_{st}[k]) - 10) \\ r_3^*(I_{st}[k]) - 0.25 \end{array} \right] \quad (6)$$

*Linear inequalities.* However, if the box has one or more corners outside the compressor limits, this is corrected using linear inequalities.

If the lower vertexes are out of the compressor working region, both vertexes are replaced by new ones. These vertexes are calculated with the polynomial regression of the lower line. This is translated to one inequality constraint.

$$n_{geq}[k]r_1[k] - r_3[k] \leq -m_{geq}[k] \quad (7)$$

where  $n_{geq}[k]$ ,  $m_{geq}[k]$  are the straight line parameters at time  $k$  for the compressor lower limit (blue line in figure 7).

For the upper boundary, the process is different. If the upper vertexes are outside the working region, a tangent line to the surge line on the left side is found in the intersection of the surge line and lower boundary of the mass flow. The tangent line is translated to one inequality constraint.

$$-n_{leq}[k]r_1[k] - r_3[k] \leq m_{leq}[k] \quad (8)$$

where  $n_{leq}[k]$ ,  $m_{leq}[k]$  are the straight line parameters at time  $k$  for the compressor higher limit (orange line in figure 7). The previous linear inequalities can be described using  $A$  and  $B$  matrices (see equation 2), which refer to an  $r$  vector containing the two  $r_1$  references and the two  $r_3$  references within the control horizon.

$$A = \begin{bmatrix} n_{geq}[1] & 0 & -1 & 0 \\ 0 & n_{geq}[2] & 0 & -1 \\ -n_{leq}[1] & 0 & -1 & 0 \\ 0 & -n_{leq}[2] & 0 & -1 \end{bmatrix}, B = \begin{bmatrix} -m_{geq}[1] \\ -m_{geq}[2] \\ m_{leq}[1] \\ m_{leq}[2] \end{bmatrix} \quad (9)$$

### 5.3.2. NMPC Slow constraints

The constraints for MV2 are independent of each other and can be defined only with upper and lower bounds.

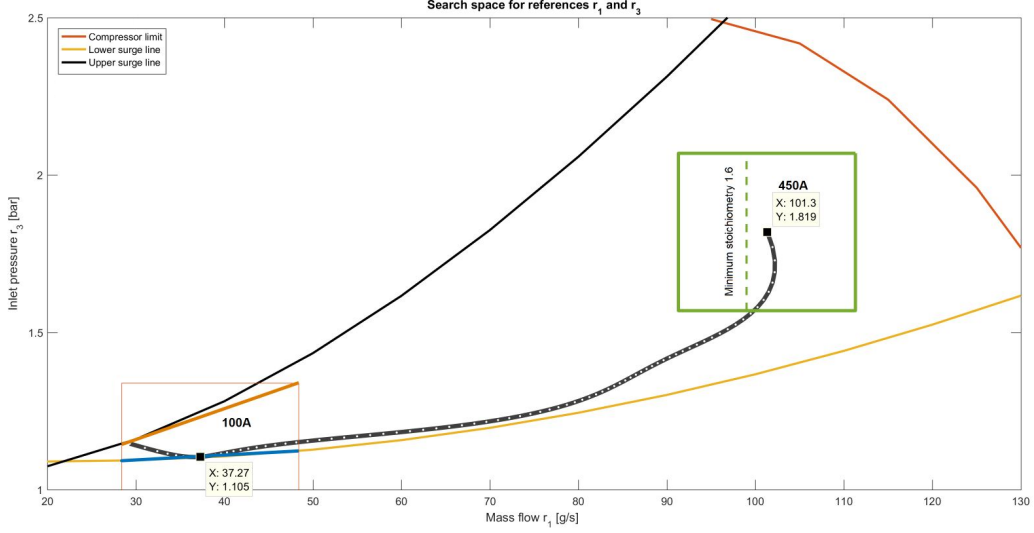


Figure 7: Example of the NMPCSlow constraints on the manipulated variables. The boxes represent the  $UB_1$  and  $LB_1$ , green for the 450 A current and orange for the 100 A current. The dashed line is the minimum required stoichiometry. The lines blue and orange are the inequality constraints on  $r_1$  and  $r_3$ . The white dots represent the offline optimal setpoints for different currents, starting from the left at  $I_{st}=50$  A and ending at  $I_{st} = 450$  A.

*Upper and lower bounds.* The references  $r_2$  and  $r_6$  are the cathode humidity ratio reference and the coolant difference temperature reference.

The upper and lower bounds on the humidity ratio are static:

$$0 \leq r_2[k] \leq 0.5 \quad (10)$$

The bound on the temperature reference, however, is to enforce the search of the optimal solution inside the working region of the thermal subsystem:

$$P_{thermal,Low}(I_{st}[k]) \leq r_6[k] \leq P_{thermal,High}(I_{st}[k]) \quad (11)$$

where  $P_{thermal,Low}(I_{st})$  and  $P_{thermal,High}(I_{st})$  are an interpolation of the high and low values that define the boundaries of the working region for a given current.

$$UB_2[k] = [0.5, P_{thermal,High}(I_{st}[k])]^T \quad (12)$$

$$LB_2[k] = [0.0, P_{thermal,low}(I_{st}[k])]^T \quad (13)$$

Table 7: Main parameters of the predictive controllers

	NMPCFast	NMPCSlow
Control time step [s], $T_s$	0.1	2
Control Horizon [s], N	0.2	10
Prediction Horizon [s], M	1	300
Total number of MV	4	10
Average computation time [s]	0.13009	0.791316
Std. deviation	0.09179	0.35875

#### 5.4. Computational time performance

The two nonlinear predictive controllers run an optimization at each time step to find the optimal references within the constraints. An analysis of the optimisation time is required to check that the controller can be run on real time. Table 7 gathers the basic configuration parameters of the model predictive controllers and the average computation times with their standard deviation for 1000 optimisations. It can be seen that the optimisation time is about 30% larger than the step time for the NMPCFast.

## 6. Controllers Comparison

The New European Driving Cycle collects velocity and acceleration profiles of representative vehicles. It can be found in the literature for simulation based analysis [12] [28]. Based on these profiles, the estimated power consumption and required stack current are computed.

The Simulink blocks used to compute the power consumption and required stack current are shown in Figure 8. The power consumption is assumed with a drag coefficient of 0.4 and a vehicle mass of two tons. Only positive accelerations are taken into account. The total force applied to the car is the mass multiplied by the acceleration plus the drag force. The power is calculated as the total force multiplied by the velocity. Then, a first order filter with unitary static gain is applied to obtain the power that has to be supplied by the fuel cell at each moment, because the fast changes are assumed to be covered by the battery. An efficiency of 25% is considered from the fuel cell to the effective torque on the motors. Finally, a saturation block is placed to set the minimum current to 60A.

The NEDC acceleration and velocity profiles are shown in Figure 9. The first part of the NEDC represents urban driving in the rush hour with four

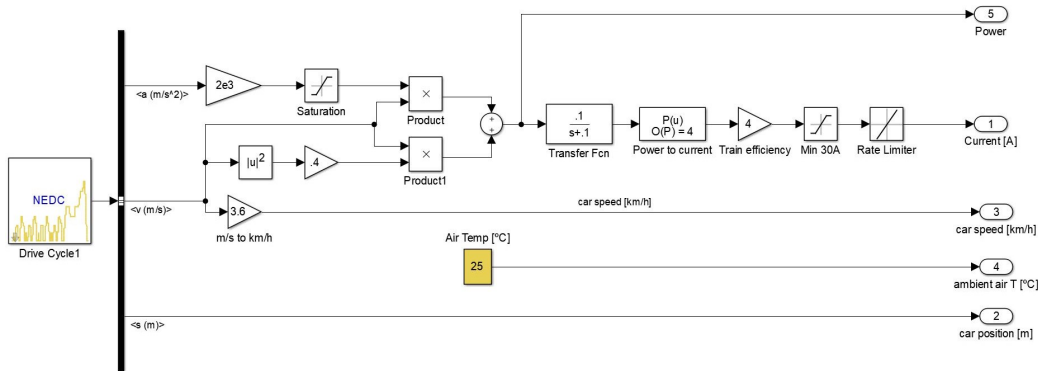


Figure 8: Stack current calculation from the NEDC

cycles of 195 seconds. Then, the seconds from 780 to 1200 represent the highway part of the journey with an average velocity of  $60 \text{ kmh}^{-1}$  and a peak of  $120 \text{ kmh}^{-1}$ . The estimated corresponding required power and current are also presented in Figure 9.

*Initial Conditions of the simulations.* For the simulation, it is assumed that the vehicle has just been turned on, the STARTUP process has finished and the state machine is in RUN mode. Besides, the ambient temperature is 25 degrees Celsius and the initial condition of the PEMFC temperature is 35 degrees after the STARTUP. The compressor is already running and delivering  $20 \text{ gs}^{-1}$  of air. The cathode is completely dry after the startup and thus the humidification is the ambient one.

### 6.1. Predictive controllers I and II

Even though only two setpoints generators have been described in the previous sections, a second predictive controller configuration is also evaluated. The new introduced predictive controller, *predictive controller I*, is a mix of the offline setpoint generator and the original predictive controller presented in the Nonlinear MPC section, named *predictive controller II*.

The *predictive controller I* calculates the setpoints of the fast dynamics from the NMPCFast optimizer and takes the setpoints for the slow dynamics from the offline setpoint generator.

Therefore, three different control configurations will be executed and compared under the NEDC:

1. Offline setpoint generator, for  $(r_1, r_2, r_3, r_6)$

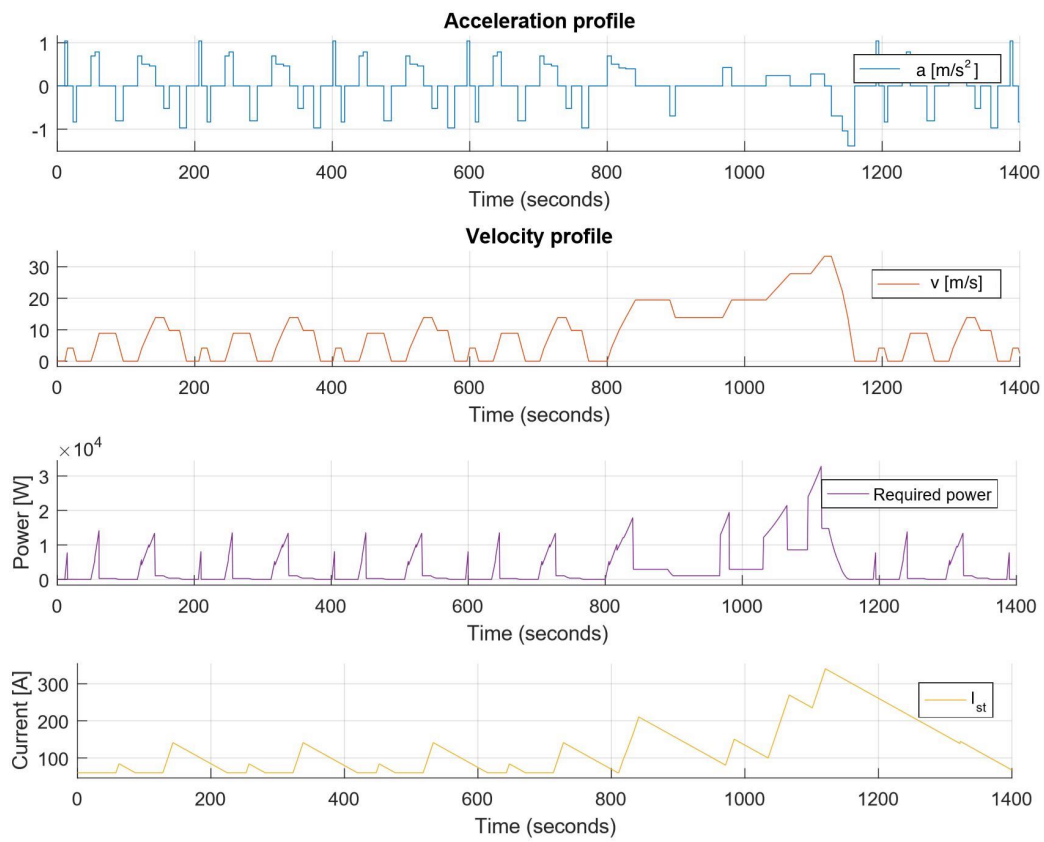


Figure 9: From top to down: NEDC velocity and acceleration, required power and required current. The cycle length is 1200 seconds.

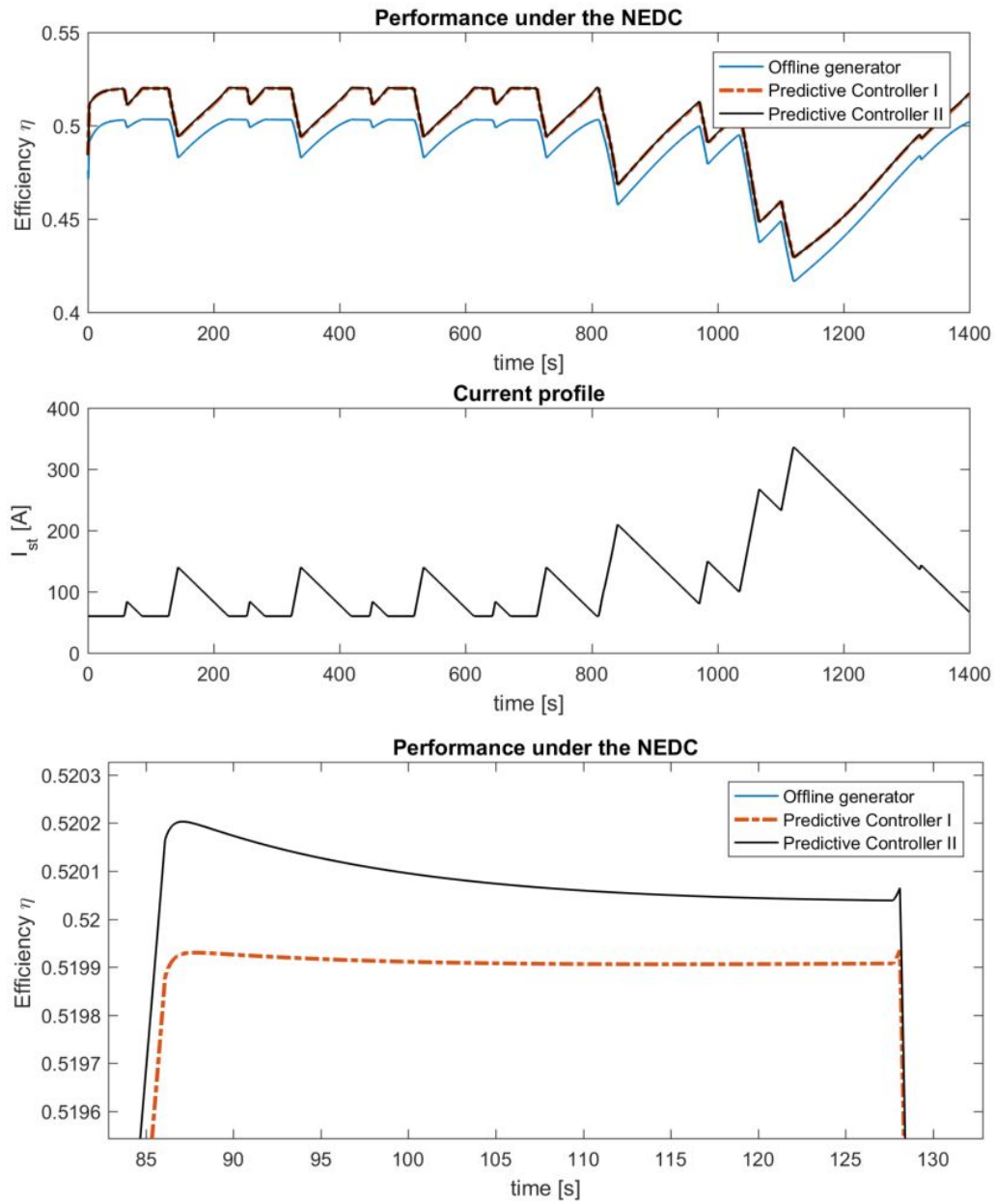


Figure 10: Performance of the setpoint generators under the NEDC

2. *Predictive controller I*: NMPCFast for  $(r_1, r_3)$  + offline setpoint generator for  $(r_2, r_6)$
3. *predictive controller II*: NMPCFast for  $(r_1, r_3)$  + NMPCSlow for  $(r_2, r_6)$ .

### 6.2. Simulation results

The performance of the three controllers can be observed in figure 10. The first two graphs show the efficiency and the current profile for the total extension of the simulation, and the third one is a zoom into the efficiency graph to appreciate the differences between the predictive controllers.

The offline setpoint generator has the lowest efficiency and the *predictive controller II* has the highest. At low currents, the offline setpoint generator is around 4% less efficient than the predictive controllers, however, at higher currents, the results are closer. It can be seen that despite *predictive controller I* is simpler than *II*, it is already a better solution than the offline setpoint generator. It can also be observed that the efficiency changes are slower for the offline setpoint generator than for the predictive controllers. It should be noted that the exact efficiency would be lower if all the minor auxiliary consumptions assumed constant were considered. However, this would not affect the found optimal setpoints neither the efficiency comparative analysis of the different controllers.

A more noticeable and interesting result is the similar performance of *predictive controller I* and *predictive controller II*. This is due to the fact that the cathode subsystem dynamics plays a significant role in the PEMFC system, and both predictive controllers consider it. In the third plot of Figure 10 it can be seen that the *predictive controller II* has a slightly higher efficiency, what happens over the whole simulation. The reason is that this predictive controller uses a more complete model.

*Control actions.* The four control actions of the three controllers are shown in Figure 11. The predictive controllers *I* and *II* found almost the same mass flow and pressure optimal references. The offline setpoint generator operates at higher mass flows and higher pressures. The humidity ratio reference plot shows a significant difference between the offline and the *predictive controller II*. The *predictive controller I* gives the same reference as the offline setpoint generator. The *predictive controller II* adjusts the humidity ratio reference based on the actual water content on the humidifier which is increasing slowly but steadily in the journey. In spite of the different humidity references, the

two predictive controllers give similar performance. *Predictive controller II* also sets the temperature reference,  $r_6$ , higher compared to the others.

### 6.3. Comparison conclusion

It can be concluded that all three controllers are inside the standards with similar performance. With none of the complexity of the predictive controllers, the offline setpoint generator is able to manage the load achieving efficiencies up to 50%. The *predictive controllers I* and *II* show greater efficiency for all the range of currents. There is no clear benefits of implementing the more complex predictive controller, *predictive controller II*, over the one that takes into account only the fast dynamics, *predictive controller I*. The increase in complexity does not go together with significantly higher performance. It is relevant to highlight the *predictive controller I*, which optimizes the mass flow and pressure references and leaves the slow dynamics of humidification and temperature dependant to the offline setpoint generator.

## 7. Conclusions and future work

In this work, a successful comparison of three PEMFC setpoint generators has been carried out using the NEDC velocity profile. One is based on the static offline map of the system efficiency and the other two are model predictive controllers that use low order models of the system.

The evaluation of the three controllers yields clear results. All three controllers satisfy all system restrictions and are implementable in a real system. A further analysis indicates that the two dynamic controllers always perform better than the static controller. The comparison shows an improvement margin in the system efficiency up to 4%.

There is a trade off between the system efficiency achieved by the controllers and their computational complexity. In this trade off, *predictive controller I* is the most interesting option due to its simplicity with almost the same performance as *predictive controller II*.

It is also worth noticing that the computational time necessary for the predictive controllers to calculate the control actions are not yet inside the limit to be deployed. The average time for the control action computation for the predictive controllers is 30% larger than the step time defined. In the future, the controllers will be translated from MATLAB/Simulink to C++ to be embedded in a control unit with higher computational power. Moreover, we believe that there is further room for improvements. For instance, further

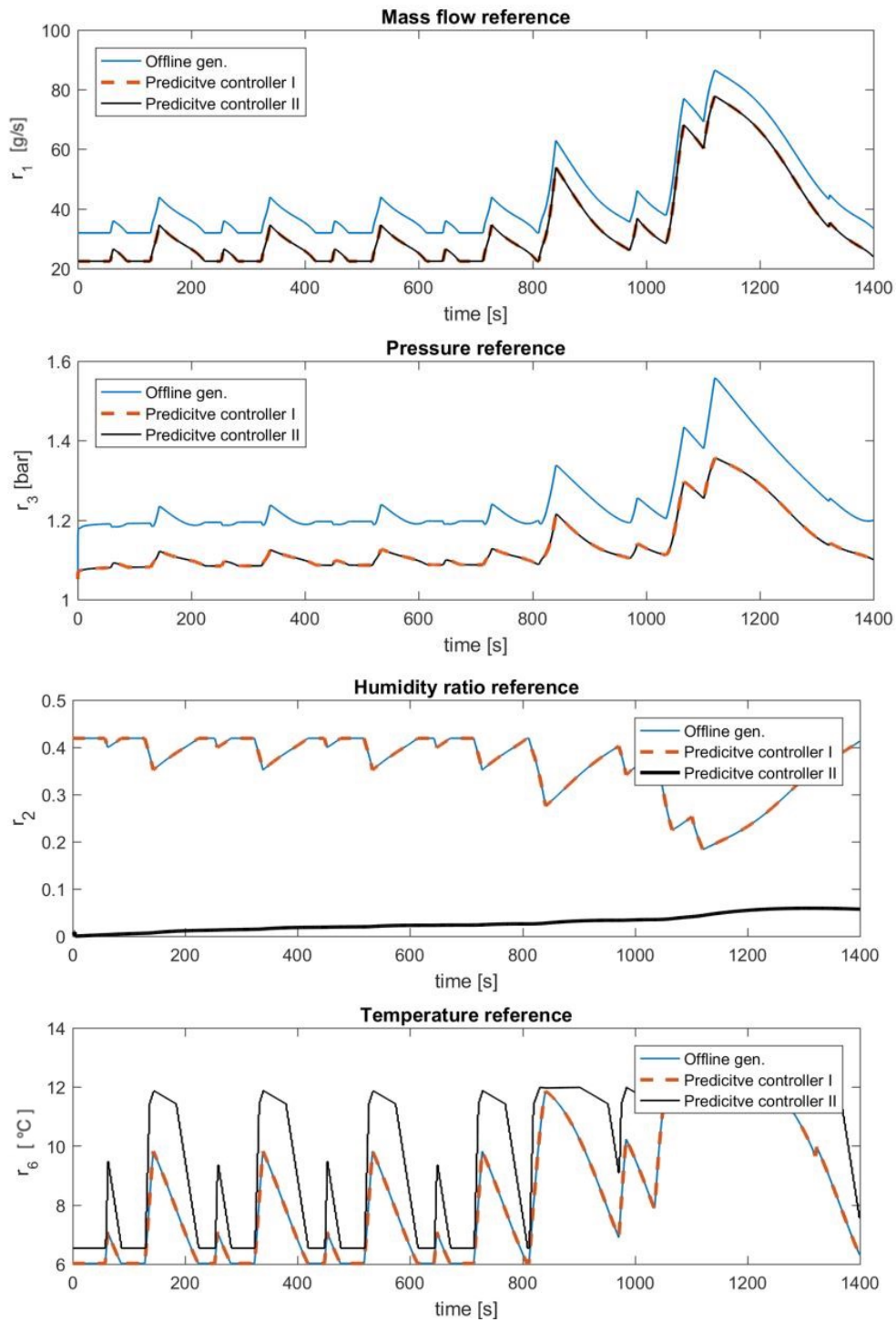


Figure 11: Generated references  
31

work can include improving the internal models of the predictive controllers using piece-wise linear models with the exact time-discretization method. This would reduce significantly the computational cost. Furthermore, the proposed supervisory controllers should be tested with other driving cycles, such as the Worldwide Harmonized Light Vehicles Test Procedure (WLTP), which has become a global standard for light duty vehicles.

## 8. Acknowledgements

This work was supported in part by the Spanish national project DOVELAR (RTI2018-096001-B-C32, MINECO/FEDER) also in part by the Spanish State Research Agency through the María de Maeztu Seal of Excellence to IRI (MDM-2016-0656), and finally in part by the Fuel Cells and Hydrogen 2 Joint Undertaking under Grant INN-BALANCE 735969. This Joint Undertaking receives support from the European Union’s Horizon 2020 research and innovation program and Hydrogen Europe and N.ERGHY.

## References

- [1] F. Barbir, *PEM Fuel Cells: theory and practice*. Elsevier, 2014.
- [2] “Inn-balance project description,” <https://www.innbalance-fch-project.eu/>, accessed: 2019-06-11.
- [3] W. Daud, R. Rosli, E. Majlan, S. Hamid, R. Mohamed, and T. Husaini, “Pem fuel cell system control: A review,” *Renewable Energy*, vol. 113, pp. 620–638, 2017.
- [4] F. Wang and C. Ko, “Multivariable robust pid control for a pemfc system,” *International Journal of Hydrogen Energy*, vol. 35, no. 19, pp. 10 437–10 445, 2010.
- [5] F. Tiss, R. Chouikh, and A. Guizani, “Dynamic modeling of a pem fuel cell with temperature effects,” *International Journal of Hydrogen Energy*, vol. 38, no. 20, pp. 8532–8541, 2013.
- [6] H. Yuan, H. Dai, X. Wei, and P. Ming, “Model-based observers for internal states estimation and control of proton exchange membrane fuel cell system: A review,” *Journal of Power Sources*, vol. 468, p. 228376, 2020.

- [7] Y. Xing, J. Na, and R. Costa, “Real-time adaptive parameter estimation for a polymer electrolyte membrane fuel cell,” *IEEE Transactions on Industrial Informatics*, vol. 15, no. 11, pp. 6048–6057, 2019.
- [8] M. Sarmientoa, M. Serra, and C. Batlle, “Distributed parameter model-based control of water activity and concentration of reactants in a polymer electrolyte membrane fuel cell,” *International Journal of Hydrogen Energy*, vol. 42, pp. 26 389–26 407, 2017.
- [9] C. Ziogou, S. Papadopoulou, M. C. Georgiadis, and S. Voutetakis, “On-line nonlinear model predictive control of a pem fuel cell system,” *Journal of Process Control*, vol. 23, no. 4, pp. 483–492, 2013.
- [10] C. Ziogou, S. Voutetakis, M. Georgiadis, and S. Papadopoulou, “Model predictive control (mpc) strategies for pem fuel cell systems – a comparative experimental demonstration,” *Chemical Engineering Research and Design*, vol. 131, pp. 656–670, 2018.
- [11] J. Luna, S. Jemei, N. Yousfi-Steiner, A. Husar, M. Serra, and D. Hissel, “Nonlinear predictive control for durability enhancement and efficiency improvement in a fuel cell power system,” *Journal of Power Sources*, vol. 328, pp. 250–261, 2016.
- [12] J. Luna, E. Usai, A. Husar, and M. Serra, “Enhancing the efficiency and lifetime of a proton exchange membrane fuel cell using nonlinear model predictive control with nonlinear observation,” *IEEE Transactions on Industrial Electronics*, vol. 64, no. 8, pp. 6649–6659, 2017.
- [13] J. Lu and A. Zahedi, “Predictive control of pemfc based on a combined empirical and mechanistic model,” *IEEE International Conference on Power System Technology (POWERCON), Auckland, New Zealand*, pp. 1–6, 2012.
- [14] S. Cheng, L. Xu, J. Li, C. Fang, J. Hu, and M. Ouyang, “Development of a pem fuel cell city bus with a hierarchical control system,” *Energies*, vol. 9, no. 6, p. 417, 2016.
- [15] W. Zhang, J. Li, L. Xu, and M. Ouyang, “Optimization for a fuel cell/battery/capacity tram with equivalent consumption minimization strategy,” *Energy Conversion and Management*, vol. 134, pp. 59–69, 2017.

- [16] C. Lin, M. Kim, H. Peng, and J. Grizzle, “System-level model and stochastic optimal control for a pem fuel cell hybrid vehicle,” *Journal of Dynamic Systems, Measurement, and Control*, vol. 128, no. 4, pp. 878–890, 2006.
- [17] T. Fletcher, R. Thring, and M. Watkinson, “An energy management strategy to concurrently optimise fuel consumption and pem fuel cell lifetime in a hybrid vehicle,” *International Journal of Hydrogen Energy*, vol. 41, no. 46, pp. 21 503–21 515, 2016.
- [18] T. Fletcher and K. Ebrahimi, “The effect of fuel cell and battery size on efficiency and cell lifetime for an l7e fuel cell hybrid vehicle,” *Energies*, vol. 13, no. 22, p. 5889, 2020.
- [19] J. Wu, N. Zhang, D. Tan, and J. C. W. Shi, “A robust online energy management strategy for fuel cell/battery hybrid electric vehicles,” *International Journal of Hydrogen Energy*, vol. 45, no. 27, pp. 14 093–14 107, 2020.
- [20] M. Mangold, A. Bück, and R. Hanke-Rauschenbach, “Passivity based control of a distributed pem fuel cell model,” *Journal of Process Control*, vol. 20, pp. 292–313, 2010.
- [21] J. Luna, A. Husar, and M. Serra, “Nonlinear distributed parameter observer design for fuel cell systems,” *International Journal of Hydrogen Energy*, vol. 40, no. 34, pp. 11 322–11 332, 2015.
- [22] M. Wöhr, K. Bolwin, W. Schnurnberger, M. Fischer, W. Neubrand, and G. Eigenberger, “Dynamic modelling and simulation of a polymer membrane fuel cell including mass transport limitation,” *International Journal of Hydrogen Energy*, vol. 23, no. 3, p. 212–218, 1998.
- [23] S. Strahl, A. Husar, P. Puleston, and J. Riera, “Performance improvement by temperature control of an open cathode pem fuel cell system,” *Fuel Cells*, vol. 14, no. 3, pp. 466–478, 2014.
- [24] V. Liso, M. P. Nielsen, S. K. Kær, and H. H. Mortensen, “Thermal modeling and temperature control of a pem fuel cell system for forklift applications,” *International Journal of Hydrogen Energy*, vol. 39, no. 16, pp. 8410–8420, 2014.

- [25] J. Gomez, M. Serra, and A. Husar, “Pem automotive stack model with experimental validation,” *VII Iberian Symposium on Hydrogen, Fuel Cells and Advanced Batteries*, pp. 238–241, Barcelona, 2019.
- [26] L. Boyd, Stephen P; Vandenberghe, *Convex optimization*. Cambridge: Cambridge University Press, 2004.
- [27] L. Wang, *Model Predictive Control System Design and Implementation Using MATLAB*. Advancements in Industrial Control, 2009.
- [28] M. Mayur, S. Strahl, A. Husar, and W. Bessler, “A multi-timescale modeling methodology for pemfc performance and durability in a virtual fuel cell car,” *International Journal of Hydrogen Energy*, vol. 40, no. 46, pp. 16 466–16 476, 2015.